J|A|C|S
ARTICLES
Published on Web 08/10/2005

Kinetic and Spectroscopic Characterization of ACMSD from *Pseudomonas fluorescens* Reveals a Pentacoordinate Mononuclear Metallocofactor

Tingfeng Li,[†] Antoinette L. Walker,[†] Hiroaki Iwaki,[‡] Yoshie Hasegawa,[‡] and Aimin Liu*,[†]

Contribution from the Department of Biochemistry, University of Mississippi Medical Center, Jackson, Mississippi 39216-4505, and Department of Biotechnology, Faculty of Engineering, Kansai University, Suita, Osaka 564-8680, Japan

Received May 17, 2005; E-mail: aliu@biochem.umsmed.edu

Abstract: The enzyme α-amino-β-carboxy-muconic-ε-semialdehyde decarboxylase (ACMSD) plays an important role in the biodegradation of 2-nitrobenzoic acid in microorganisms and in tryptophan catabolism in humans. We report that the overexpressed ACMSD enzyme from *Pseudomonas fluorescens* requires a divalent metal, such as Co(II), Fe(II), Cd(II), or Mn(II), for catalytic activity and that neither a redox reagent nor an organic cofactor is required for the catalytic function. The metal ions can be taken up in either cell or cell-free preparations for generating the active form of ACMSD. The kinetic parameters and enzyme specific activity are shown to depend on the metal ion present in the enzyme, suggesting a catalytic role of the metal center. EPR spectrum of Co(II)-ACMSD provides a high-spin ($S = {}^3/_2$) mononuclear metal ion in a non-heme, noncorrinoid environment with a mixed nitrogen/oxygen ligand field. We observe hyperfine interactions due to ^{59}Co nucleus at temperatures below 5 K but not at higher temperatures. Ten hyperfine lines are present in the $g_\perp$ region, and three equivalent nitrogen hyperfine couplings are required to simulate the resonances in the EPR spectrum. The results for the metal binding site are also assessed using the copper-substituted enzyme, and the EPR spectral assignments for both cobalt and copper proteins give strong support for a distorted trigonal bipyramidal geometry of the metal center. Ultimately, these results suggest for the first time that ACMSD is a metal-dependent enzyme that catalyzes a novel nonoxidative decarboxylation.

Introduction

The decarboxylation of α-amino-β-carboxy-muconic-ε-semialdehyde (**4**, ACMS) has been studied for nearly 50 years.[1−4] More than four decades after the first isolation of the obligatory decarboxylase enzyme, ACMSD,[3−5] neither the enzyme cofactor nor the mechanisms of this important decarboxylase are known. The ACMS decarboxylation plays an important role in two natural metabolic pathways, i.e., 2-nitrobenzoic acid (**1**) biodegradation in bacteria and L-tryptophan (**2**) catabolism in mammals (Scheme 1). This reaction is a key control that directs the metabolic stream to acetyl CoA for energy production rather than accumulation of excitotoxin quinolinic acid (**6**, QUIN). ACMSD has been purified from various sources, indicating that it is widely spread in biological systems.[4−9] The protein sequences from the above two metabolic pathways share a high degree of similarity. Due to the instability of both the substrate (**4**) and the immediate product 2-aminomuconic-6-semialdehyde (AMS, **5**), investigation of this decarboxylation reaction and chemical mechanism is surprisingly challenging.

Research in recent years has established that 3-hydroxyanthranilate (**3**) is the precursor of **4**. This is the first common reaction intermediate detectable in both of the above metabolic events. It is also the last intermediate prior to the ring breaking in the nitrobenzoic acid biodegradation process. A non-heme Fe enzyme, 3-hydroxyanthranilate-3,4-dioxygenase (HAD), efficiently converts **3** to **4** in an O_2-dependent process.[6,10,11] Then the reaction cascade arrives at a branch point from which an enzyme, namely ACMS decarboxylase (ACMSD), directs the

[†] University of Mississippi Medical Center.
[‡] Kansai University.

(1) Abbreviations used: ACMS, α-amino-β-carboxy-muconic-ε-semialdehyde; ACMSD, α-amino-β-carboxy-muconic-ε-semialdehyde decarboxylase or 2-amino-3-carboxymuconate-6-semialdehyde (EC 4.1.1.45); AMS, 2-aminomuconic-6-semialdehyde; 3-HAA, 3-hydroxyanthranilic acid; HAD, 3-hydroxyanthranilate 3,4-dioxygenase; HEPES, 4-(2-hydroxymethyl)-1-piperazineethanesulfonic acid; 2-NBA, 2-nitrobenzoic acid; QUIN, quinolinic acid.

(2) May, E. L.; Mehler, A. H. *J. Biol. Chem.* **1956**, *223*, 449−455.
(3) Mehler, A. H. *J. Biol. Chem.* **1956**, *218*, 241−254.
(4) Nishizuka, Y.; Ichiyama, A.; Hayaishi, O. *Methods Enzymol.* **1970**, *266*, 463−466.
(5) Nishizuka, Y.; Ichiyama, A.; Gholson, R. K.; Hayaishi, O. *J. Biol. Chem.* **1965**, *240*, 733−739.
(6) Muraki, T.; Taki, M.; Hasegawa, Y.; Iwaki, H.; Lau, P. C. *Appl. Environ. Microbiol.* **2003**, *69*, 1564−1572.
(7) Fukuoka, S.; Ishiguro, K.; Yanagihara, K.; Tanabe, A.; Egashira, Y.; Sanada, H.; Shibata, K. *J. Biol. Chem.* **2002**, *277*, 35162−35167.
(8) Egashira, Y.; Kouhashi, H.; Ohta, T.; Sanada, H. *J. Nutr. Sci. Vitaminol.* **1996**, *42*, 173−183.
(9) Tanabe, A.; Egashira, Y.; Fukuoka, S.; Shibata, K.; Sanada, H. *Biochem. J.* **2002**, *361*, 567−575.
(10) Colabroy, K. L.; Zhai, H.; Li, T.; Ge, Y.; Zhang, Y.; Liu, A.; Ealick, S. E.; McLafferty, F. W.; Begley, T. P. *Biochemistry* **2005**, *44*, 7623−7631.
(11) Zhang, Y.; Colabroy, K. L.; Begley, T. P.; Ealick, S. E. *Biochemistry* **2005**, *44*, 7632−7643.

10.1021/ja0532234 CCC: $30.25

Scheme 1. Enzyme ACMSD Plays a Key Role in the Shared Steps of Two Unrelated Metabolic Events, i.e., 2-NBA Biodegradation in Bacteria (A) and a Fundamental Tryptophan Catabolic Pathway in Humans (B)

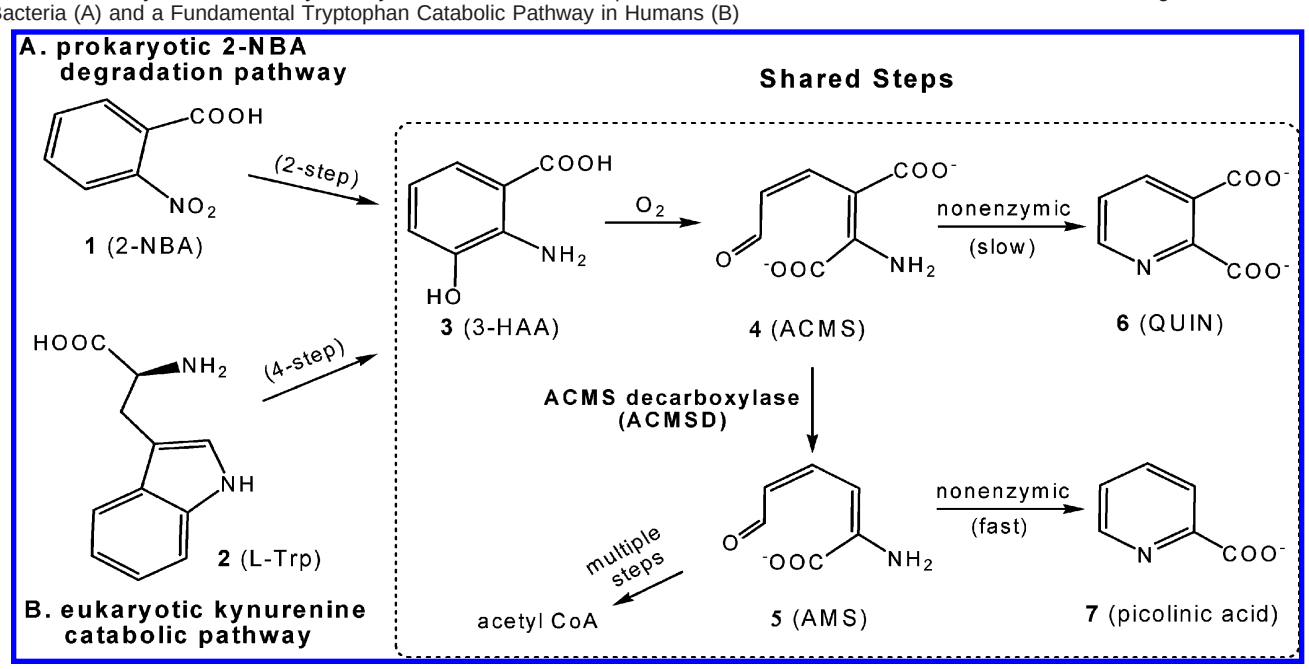

flux to either acetyl CoA for energy production in the citric acid cycle or **6** in a spontaneous but slow pericyclic reaction process.[12] QUIN is a potent endogenous excitotoxin of neuronal cells in humans.[13] It excites neurons in the central nervous system by acting as a selective activator of certain glutamate receptors that are sensitive to *N*-methyl-D-aspartate.[14−16] Excessive accumulation of **6** can lead to cell death.[16,17] In fact, elevated levels of **6** in body fluids are observed in an exceptionally wide range of neuropsychiatric disease states, including anxiety, depression, and epilepsy, as well as neurodegenerative diseases, such as Alzheimer's and Huntington's diseases.[14,16,18] During excess protein dietary intake, tryptophan's kynurenine pathway is the major route of catabolism when this amino acid is used other than as a protein building block. Thus, the branch point partitioned by ACMSD is an important control in this eukaryotic metabolic pathway.

On the biodegradation pathway, **1** is a precursor of numerous toxic compounds in the environment. It irritates the eyes, respiratory system, and skin and possesses some carcinogenic effects.[19] For environmental preservation, the biodegradation of toxic and persistent pollutants such as **1** is a noteworthy process. Like in the other pathway, the enzyme activity of bacterial ACMSD is critical for the committed step to direct the biodegradation stream for complete oxidation and energy production.

In the present study, we describe a biochemical and spectroscopic study of ACMSD from *Pseudomonas fluorescens*. This is the only decarboxylase enzyme in the bacterial 2-nitrobenzoic acid biodegradation pathway that has been identified thus far.[6] This bacterial enzyme shares a higher degree of sequence similarities with the eukaryotic counterparts. Our work described in this report attests that the bacterial ACMSD contains a catalytic mononuclear metal center, and such a metal cofactor dependency is unprecedented for a nonoxidative decarboxylation. These findings have important implications for understanding the human ACMSD mechanism.

Experimental Procedures

Protein Preparations. The nonheme Fe(II) enzyme HAD was prepared for the coupled assay according to the procedures described in earlier reports.[6,20] DNA manipulation and cloning of ACMSD has been described earlier.[6] For ACMSD preparation, *E. coli* strains BL21-(DE3) encoding the full length ACMSD expression construct pACMSD1 was inoculated into autoclaved Luria−Bertani (LB) medium containing 100 μg/mL ampicillin. A culture was grown overnight at 37 °C with agitation, and a 6-L batch culture was further inoculated and grown to 0.4 O.D. ($A_{595\ nm}$) at 37 °C. The temperature was lowered to 28 °C and isopropyl-β-D-thiogalactopyranoside was added to a final concentration of 1 mM at ca. 0.6 O.D. followed by addition of 0, 200, or 500 μM $CoCl_2$ in different sets of experiments. The culture was allowed to grow continuously for an additional 4 h at 28 °C before harvest. The frozen cells containing overexpressed ACMSD were resuspended in a 50 mM potassium phosphate buffer, pH 7.0, containing 10 mM β-mercaptoethanol, 1 mM phenylmethylsulfonyl fluoride, and 0.1 mg/mL lysozyme. The cell slurry was sonicated, and the debris was removed by centrifugation at 27 000 × *g* for 30 min at 4 °C. Ammonium sulfate was added to fraction the supernatant. The precipitated protein with 40−60% saturation of ammonium sulfate was resuspended in a minimal amount of 50 mM potassium phosphate buffer, pH 7.0, containing 10 mM β-mercaptoethanol and 10% glycerol, then loaded onto a G-50 column (Amersham) and eluted with the same buffer. Fractions containing protein with ACMSD activity were pooled and loaded onto a DEAE (DE-52) column (Whatman) and eluted with a linear gradient of 0.1−0.5 M NaCl in the same buffer. The major fraction possessing ACMSD activity was pooled and dialyzed against

(12) Colabroy, K. L.; Begley, T. P. *J. Am. Chem. Soc.* **2005**, *127*, 840−841.
(13) Schwarcz, R.; Whetsell, W. O., Jr.; Mangano, R. M. *Science* **1983**, *219*, 316−318.
(14) Schwarcz, R. *Curr. Opin. Pharmacol.* **2004**, *4*, 12−17.
(15) Stone, T. W.; Mackay, G. M.; Forrest, C. M.; Clark, C. J.; Darlington, L. G. *Clin. Chem. Lab. Med.* **2003**, *41*, 852−859.
(16) Stone, T. W.; Darlington, L. G. *Nat. Rev. Drug Discov.* **2002**, *1*, 609−620.
(17) Mellor, A. L.; Munn, D. H. *J. Immunol.* **2003**, *170*, 5809−5813.
(18) Schwarcz, R.; Okuno, E.; White, R. J.; Bird, E. D.; Whetsell, W. O., Jr. *Proc. Natl. Acad. Sci. U.S.A.* **1988**, *85*, 4079−4081.
(19) Cambridgesoft *ChemMSDX* **2005**, A10393.PDF.
(20) Colabroy, K. L.; Zhai, H.; Li, T.; Ge, Y.; Zhang, Y.; Liu, A.; Ealick, S. E.; McLafferty, F. W.; Begley, T. P. *Biochemistry* **2005**, *44*, 7623−7631.

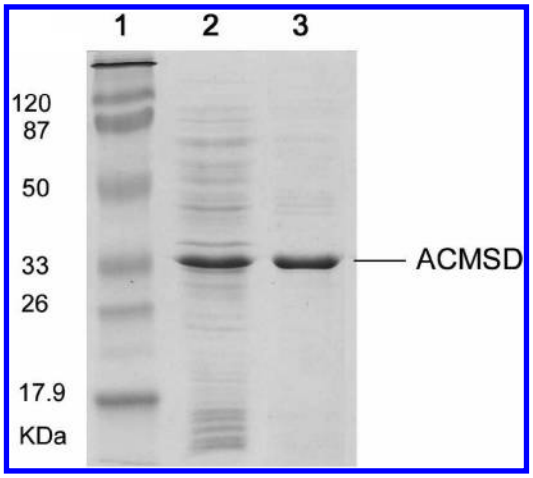

Figure 1. SDS-PAGE shows expression in the crude extract and purified ACMSD. Lane 1 molecular standards; lane 2 crude extract; and lane 3 purified protein.

a 25 mM HEPES buffer, pH 7.0, containing 10% glycerol. In the preparation of apoprotein (metal-free form), 1 mM EDTA was also included in all the buffers before loading to a DEAE column. The protein was concentrated by ultrafiltration or by using an Amicon concentrator with YM-10 membrane. For the preparation of apo-ACMSD, 1 mM EDTA was included in the initial buffer for extraction of the enzyme from cells, and the pool of the final column was mixed with 5 mM EDTA for at least 1 h before dialysis.

Protein concentration was determined by using Coomassie Plus protein assay reagent (Pierce) according to the manufacturer's protocol. The expression level and enzyme purity were determined by SDS-PAGE on 12% polyacrylamide gels (Figure 1). The molecular weight of the bacterial ACMSD, estimated from protein sequences and SDS-PAGE gel, is 39 KDa, which is nearly the same as that of the human counterpart found in the kynurenine pathway.[7]

Enzyme Activity Assay. ACMSD activity of crude cell extract and purified protein were measured in a 25 mM HEPES buffer, pH 7.0, 5% glycerol at 25 °C. In a typical assay experiment, the appropriate amount of Fe(II)-containing HAD and **3** were used to generate an expected amount of **4** ($\epsilon_{360\ nm} = 47\ 500\ M^{-1}\ cm^{-1}$),[21] i.e., the substrate of ACMSD. ACMS was rapidly formed, and its characteristic absorbance at 360 nm was followed by optical spectrum on an Agilent 8453 spectrophotometer. When the reaction was completed, the cell-free extract or the purified protein of ACMSD was immediately added into the assay system followed by monitoring the decrease of absorbance at 360 nm (i.e., the decay of **4**). No free Fe(II) ion was added to the entire assay system. The initial velocity was calculated from data of the first 10 s and subtracted from that of the control reaction mixture without ACMSD. When divalent metals were used to activate the enzyme, they were prepared anaerobically using a homemade Schlenk line.

Activation of Apoprotein by Metal Ions. $CaCl_2$, $CdCl_2$, $CoCl_2$, $CuSO_4$, $Fe(NH_4)_2(SO_4)_2$, $MgSO_4$, $MnCl_2$, $NiSO_4$, and $FeCl_3$ solutions were all freshly prepared, among which $Fe(NH_4)_2(SO_4)_2$ was prepared anaerobically. The apo-ACMSD was first reconstituted with the appropriate amount of divalent metal under the protection of argon. The reconstitution was allowed to proceed on ice for 2 h with gentle stirring under O_2-free conditions. Then the metal-recharged ACMSD was added to a freshly generated ACMS solution as described above to assess the enzyme activity either aerobically or anaerobically.

Steady-State Kinetics and Metal Specificity. Kinetic values were measured using ACMSD (reconstituted with one to two molar equivalents of divalent metal) with substrate at various concentrations (0−30 μM) and a fixed ACMSD concentration of 0.1 μM, in 25 mM HEPES buffer, pH 7.0, 5% glycerol at 25 °C. V_{max} and K_m values were obtained through the Lineweaver−Burk double reciprocal plots.

Electron Paramagnetic Resonance (EPR) Spectroscopy. Low-temperature X-band EPR first derivative spectra were recorded in perpendicular mode on a Bruker (Billerica, MA) EMX spectrometer at 100-kHz modulation frequency using a 4119HS high-sensitivity resonator. Sample temperature was maintained with an ITC503S temperature controller, an ESR910 liquid helium cryostat and LLT650/13 liquid helium transfer tube (Oxford Instruments, Concord, MA). A calibrated frequency meter was used to aid the *g*-value determination. Spin concentration was determined by double integration of the sample spectrum obtained under nonsaturating conditions and comparing the resulting intensity to that of a copper standard (1 mM $CuSO_4$, 10 mM EDTA) or a $CoCl_2$ sample (1 mM in 25 mM HEPES, pH 7.0, 10% glycerol) obtained under identical conditions. Spectral baseline corrections were performed on personal computers using the WinEPR software package (Bruker). EPR simulation was accomplished by using the WEPR program developed by Dr. Frank Neese[22] and by the theoretical predictions according to the spin Hamiltonian described in SimFonia (version 1.25).[23] No assumptions were made regarding the orientations of the principal axes of *g* and *A* in the calculations.

Results

ACMSD Specific Activity Is Sensitive to Divalent Metal and EDTA. To clarify whether ACMSD utilizes any metal ion as cofactor for catalysis, extra caution was taken in our coupled enzyme assay experiments. An apparent difference between our assay conditions and previous reports is that there was no free Fe(II) ion added to the assay mixture. The ACMSD enzyme activity of the cell-free extract was increased about 15-fold when divalent metal, such as $CoCl_2$, was present in the medium during cell growth (Figure 2). When 50 μM $CoCl_2$ was directly added to the cell-free extract, the specific activity increased 20−30-folds. These results indicate that ACMSD is sensitive to metal ions and that divalent metal can be taken up in either cell or cell-free preparations. On the other hand, EDTA showed an adverse effect on the ACMSD activity. Incubation with EDTA (1 mM) for 12 h at 4 °C revoked the ACMSD activity from cell-free extracts. While in the control samples, the ACMSD activity of cell-free preparations largely retained upon storage at 4 °C, suggesting that the loss of specific activity is not due to degradation of the enzyme. These results led us to conclude that supplement of Co(II) to cell culture or crude extract can significantly increase the enzyme specific activity, whereas incubation with a metal chelator can adversely affect the enzyme activity.

Metal Ion Titration on Purified Apoenzyme. ACMSD purified in the presence of EDTA had no measurable decarboxylation activity. Metal ion titrations were conducted, and the resulting ACMSD samples were assayed. In the control experiments, metal ions alone did not decarboxylate ACMS, nor did the purified apoprotein. Loss of activity due to inclusion of EDTA in protein preparations was regained upon addition of divalent metal salts. Among the metal ions tested, Cd(II), Co(II), Fe(II), and Mn(II) were capable of generating the active form of the enzyme from apoprotein (Table 1). Co(II)-ACMSD presented the highest turnover rate under standard assay conditions, with Fe(II)-ACMSD as the second highest. Other divalent metal ions tested, including Cu(II), Ca(II), Mg(II), and

(21) Koontz, W. A.; Shiman, R. *J. Biol. Chem.* **1976**, *251*, 368−377.
(22) Neese, F.; Zumft, W. G.; Antholine, W. E.; Kroneck, P. M. H. *J. Am. Chem. Soc.* **1996**, *118*, 8692−8699.
(23) GmbH, B. B. *Win-EPR SimFonia* **1995**, 1−4 and 3−5.

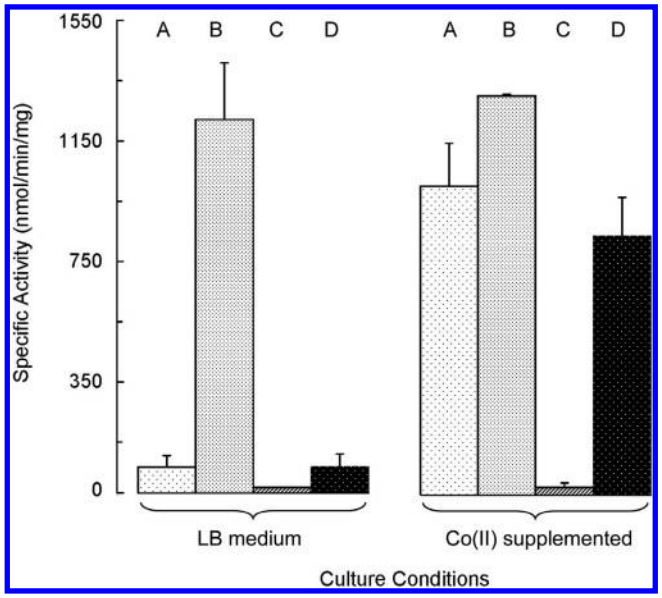

Figure 2. Effect of divalent metal and metal chelator on the decarboxylation specific activity of cell extract prepared from cells grown with LB medium (left) and LB medium supplemented with 200 μM $CoCl_2$ (right). (A) Specific activity of cell-free extract; (B) 50 μM $CoCl_2$ was incubated to the cell extract prior to assay; (C) activity after treatment by 1 mM EDTA at 4 °C for 12 h; and (D) a control cell extract sample in the same buffer as described in the text after shaking at 4 °C in the absence of EDTA for 12 h. The experiments were carried out in two media: one is a standard culture medium (left columns), and the other was supplemented with $CoCl_2$ (right columns). Errors represent standard deviation from multiple room-temperature measurements.

Table 1. Metal Cofactor Dependency, Specific Activity, and Steady State Kinetic Constants[a]

ACMSD and metal ion	specific activity (nmol/min/mg)	K_m (μM ACMS)	k_{cat} (s^{-1})	k_{cat}/K_m ($s^{-1}\,M^{-1}$) $\times 10^5$
apoprotein	inactive			
Co(II)	5900	23.2 ± 0.1	7.3 ± 0.1	3.1 ± 0.1
Mn(II)	800	6.7 ± 0.1	1.4 ± 0.1	2.1 ± 0.1
Cd(II)	1700	4.9 ± 0.1	1.7 ± 0.1	3.5 ± 0.1
Fe(II)	2900	92.1 ± 0.1	10.2 ± 0.1	1.1 ± 0.1
Fe(III)	inactive			
Cu(II)	inactive			

[a] The kinetic measurements were carried out under nonsaturating conditions due to the limitation of the high extinction coefficient of ACMS and the high turnover numbers.

Ni(II), did not activate the enzyme. Ferric ion failed to generate an active form of the enzyme, as well.

In an attempt to determine the metal/polypeptide ratio needed to fully activate the enzyme, we carried out metal ion titration and assay experiments for apo-ACMSD. 1 equiv of cobalt(II) was found to be able to restore 80−85% of the enzyme activity compared to the maximal activity observed from the same concentration of enzyme (Figure 3). 2 to 10 equiv of Co(II) per polypeptide appear to be able to fully activate the apoenzyme (Figure 3). An adverse effect was observed when more than 10-fold excess of Co(II) was added to the apoprotein. Similar results were also obtained in the Fe(II) titration/assay experiments (not shown). In these experiments, the enzyme concentration, however, was limited to a low level because of two factors. First, the high turnover numbers in our assay experiments restricted the use of enzyme at higher concentrations. Second, the substrate (**4**) possesses a high extinction coefficient ($\epsilon_{360\,nm}$ = 47 500 $M^{-1}\,cm^{-1}$),[21] and thus the substrate concentration was constrained to a range of 0−30 μM for accurate spectrophotometric analyses. These difficulties may contribute to seemingly disproportional titration results in the range of 0.5 to 2 equiv of the metal ion. Based on the 80−85% maximal enzyme activity observed from 1 equiv of divalent metal, a mononuclear metallocenter is hence proposed.

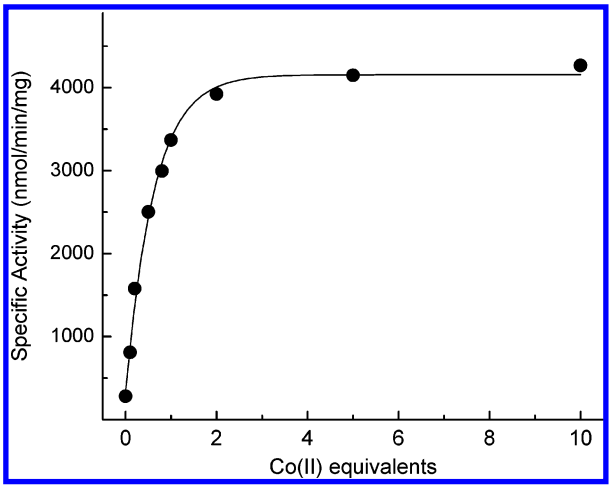

Figure 3. ACMSD activity as a function of Co(II) concentration in the titration experiment using apoprotein. The enzyme concentrations were 0.1 μM. Due to the high extinction coefficient of ACMS (47 500 $M^{-1}\,cm^{-1}$), the substrate concentration was restricted to 0−30 μM for accurate measurements. The maximal enzyme concentration was thus limited in the determination of the metal/enzyme ratio and the enzyme specific activity assays.

Steady-State Kinetics. The enzyme is activated by several different types of divalent metals. To further determine the catalytic role of the metal center and assess the catalytic efficiency of the reconstituted enzyme, a steady-state kinetic analysis was performed. Table 1 summarizes the steady-state kinetic parameters of ACMSD loaded with 1 molar equiv of Co(II), Mn(II), Cd(II), and Fe(II), respectively. The K_m value depends on the type of divalent metal used in the reconstitution reaction, spanning over a range of 5 to 92 μM, about 18-fold differences. To assess catalytic selectivity, k_{cat}/K_M values for the reconstituted enzyme samples were determined. In these experiments, Co(II)-ACMSD exhibited a high turnover rate at least one magnitude higher than that of the earlier reports, where excessive iron ion was included for the purpose of HAD activation.[2−9] However, its k_{cat}/K_m, (3.1 ± 0.1) × 10^5 $s^{-1}\,M^{-1}$, is comparable to that of the other of the reconstituted enzymes shown in Table 1. While Fe(II) is expected to be the physiologically relevant metal because of its natural abundance, it has the highest K_m. Thus, the identity of the natural metal ion for ACMSD remains to be determined in the future. Nonetheless, the above data collectively indicate that the metal ion is stoichiometrically bound at the active site and plays a catalytic role during catalysis.

Nonoxidative Decarboxylation. To decipher whether the decarboxylation is associated with an oxidant, we carried out the enzyme assay experiments under a condition free of any oxidant and organic cofactors. In this set of experiments, HAD-catalyzed 3-HAA reactions were allowed to proceed in a quartz cuvette until completion of ACMS production, which was in less than 1 min. The reaction mixture was made anaerobic by multiple rounds of gentle degassing and flushing with argon using an anaerobic gas line. Co(II)-ACMSD (O_2-free) was

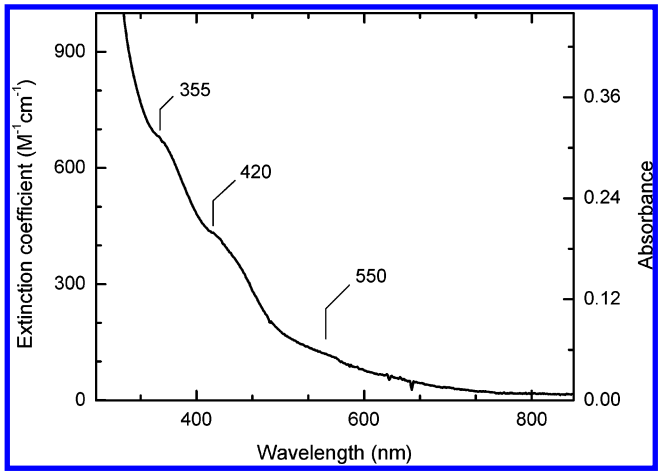

Figure 4. Electronic absorption spectrum of 460 μM ACMSD purified from LB culture supplemented with 0.5 mM $CoCl_2$ during cell growth. The metal salt was not included in the protein purification steps. The as-isolated ACMSD prepared under this condition was light brown in color at pH 7.0.

transferred into the reaction system through a gastight syringe. The decarboxylation reaction was monitored by UV−vis spectroscopy as described in the enzyme assay section. The ACMSD reaction was found to behave in the same manner as it did in the presence of O_2. The enzyme specific activity observed in the absence of an oxidant or organic cofactor is at a high level, i.e., 1 magnitude higher than that previously reported.[2−9] Although the reaction does not appear to be affected by mild chemical oxidants for the cobalt enzyme, the oxidized Fe(III)-containing enzyme was inactive. The Fe(III)-enzyme was obtained from the Fe(II)-enzyme by oxidation with pure O_2 for a few hours. Hydrogen peroxide was found to decrease the enzyme activity. These results suggest that the ACMSD reaction normally proceeds in a nonoxidative fashion.

Electronic Absorption Spectrum of Cobalt-ACMSD. ACMSD isolated from Co(II)-supplemented medium yielded three absorption bands/shoulders at 355 (680 ± 20 M^{-1} cm^{-1}), 420 (430 ± 10 M^{-1} cm^{-1}), and 550 nm (120 ± 10 M^{-1} cm^{-1}) (Figure 4). No absorbance features are presented in the Fe(II)-ACMSD, indicating that heme is not a cofactor for ACMSD. The extinction coefficient has been shown to be related to the coordination number of Co(II).[24] In general, the extinction coefficient values of the visible *d-d* band in the 450−700 nm region greater than 300 are four-coordinate, values between 50 and 300 are generally for five-coordinate, and values less than 50 are for six-coordinate. According to this empirical relationship, a pentacoordinate Co(II) in ACMSD is suggested.

EPR Characterization. The EPR spectra of Co(II)-ACMSD at 10 K display a distorted axial pattern with broad resonances that are effective for a high-spin ($S = {}^3/_2$) Co(II) center (Figure 5). The EPR signals of as-isolated cobalt-ACMSD from the LB medium supplemented with Co(II) and the Co(II) reconstituted enzyme from the apoprotein are only slightly different from each other in line shape, but they are distinct from that of free Co(II) in the same buffer. The spectrum from as-isolated ACMSD in a Co(II) supplemented medium presents some partially resolved hyperfine coupling in the low field resonance, whereas this is not seen in the reconstituted sample. Spectral

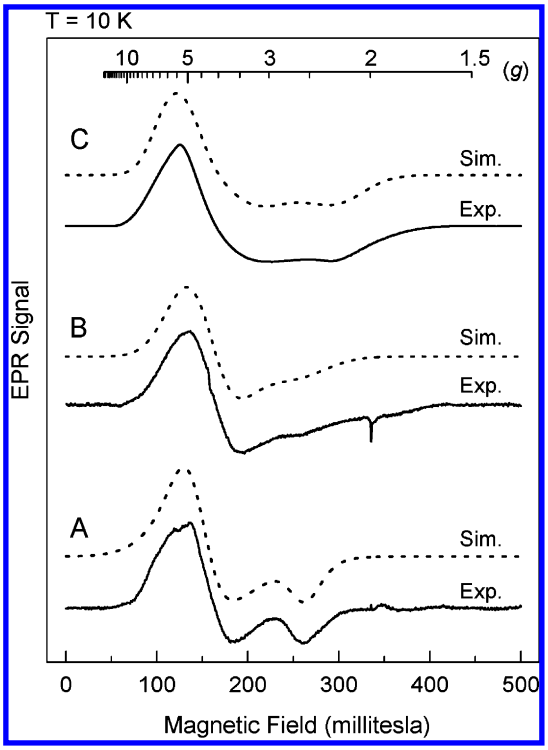

Figure 5. Frozen solution EPR spectra of cobalt(II)-ACMSD. (A) 1.2 mM as-isolated ACMSD from LB culture supplemented with 0.5 mM $CoCl_2$; (B) 0.3 mM apo-ACMSD reconstituted with 1 equiv of $CoCl_2$; and (C) 6 mM $CoCl_2$ in HEPES buffer (pH 7.0, 10% glycerol) for comparison. The *Y*-axis is the EPR first derivative amplitude presented in arbitrary scale. Simulations (Sim.) are plotted above the corresponding experimental data (Exp.). Spectrometer conditions: temperature, 10 K; modulation amplitude, 0.3 mT; microwave power, 0.5 mW; time constant, 40.96 ms; and sweep time 5.96 mT/s for the entire field between 1 and 5000 G.

simulations further reveal that a small fraction (estimated < 20%) of Co(II) in the reconstituted sample is not bound at the enzyme active site and remained as free or unspecifically bound. The exact number of free Co(II) appears to be linked with the reconstitution conditions and the concentration of the apoprotein. Nevertheless, this finding answers why 1 equiv of Co(II) represented 80−85% of the expected activity in the titration/assay experiments described above. In addition, there is a small resonance at the $g = 2$ region that arises from a trace amount of copper contaminant occasionally in some of the samples, which was observed at 10 K. The EPR data, along with the optical spectrum, are in good agreement with those of characterized Co(II) complexes with a N_3O_2 ligand set.[25] With use of the spin Hamiltonian formalism,[26] the EPR simulations were accomplished by including three equivalent nitrogen ligands. The obtained principal *g* and *A* values are given in Table 2.

The EPR spectrum of Co(II)-ACMSD is apparently resolved with a cobalt hyperfine structure at 4 K, particularly in the $g_\perp$ region, as shown in Figure 6. These hyperfine structural features are extremely fast-relaxing such that they are only visible below 5 K, a striking temperature dependency. When the sample is warmed 1 K (i.e., 6 K), the EPR signal line widths become significantly broadened. The spectrum at 6 K is essentially the same as that of 10 K as shown in Figure 5 and the multiline

(24) Seffernick, J. L.; McTavish, H.; Osborne, J. P.; de Souza, M. L.; Sadowsky, M. J.; Wackett, L. P. *Biochemistry* **2002**, *41*, 14430−14437.

(25) Chen, Y.-Y.; Chu, D. E.; McKinney, B. D.; Willis, L. J.; Cummings, S. C. *Inorg. Chem.* **1981**, *20*, 1885−1892.

(26) Weil, J. A.; Bolton, J. R.; Wertz, J. E. *Electron paramagnetic resonance: elementary theory and practical applications*; Wiley: 1994.

Table 2. EPR Parameters Obtained from Spectral Simulations for Co(II)- and Cu(II)-Containing ACMSD in Figures 5 and 8[a]

	as-isolated Co(II)-ACMSD	free Co(II) in buffer	Cu(II)-substituted ACMSD
g_x	2.6130	2.2770	2.0677
g_y	4.6491	3.6957	2.0732
g_z	4.6896	5.3530	2.2385
$A_{x(Co/Cu)}$	21.6	34.8	30
$A_{y(Co/Cu)}$	29.6	26.8	128
$A_{z(Co/Cu)}$	339.41	428.9	568
$A_{x(N)}$	3 × 21.3	0	3 × 20
$A_{y(N)}$	3 × 16.7	0	3 × 20
$A_{z(N)}$	3 × 79.1	0	3 × 25

[a] Hyperfine couplings are present in MHz; ACMSD EPR signals were simulated with three nitrogen ligands as discussed in the text.

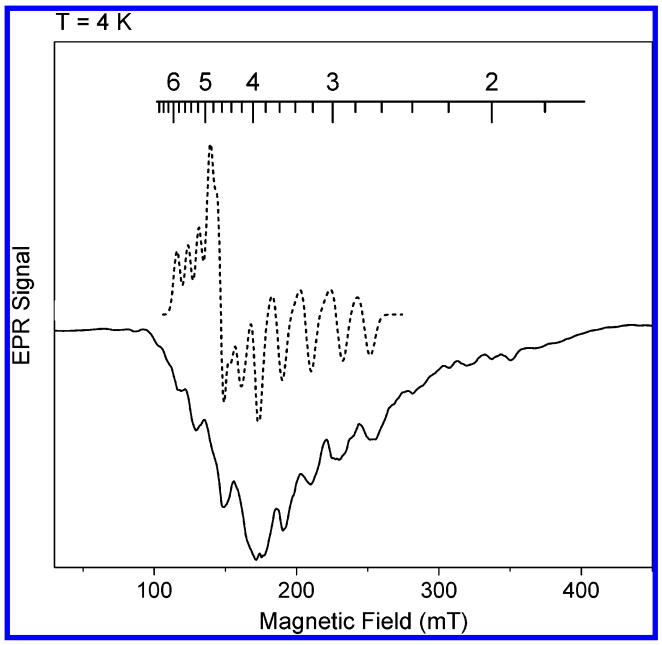

Figure 6. Low temperature (4 K) EPR spectrum of ACMSD (1.2 mM) isolated from LB medium supplemented with 0.5 mM $CoCl_2$. A calculated hyperfine structure using the simulated A and g values from the 10 K spectrum is given on top of the experimental data. Spectrometer conditions: microwave frequency, 9.38 GHz; modulation amplitude, 0.3 mT; microwave power, 0.05 mW; time constant, 327.68 ms; and sweep time 10.49 mT/s.

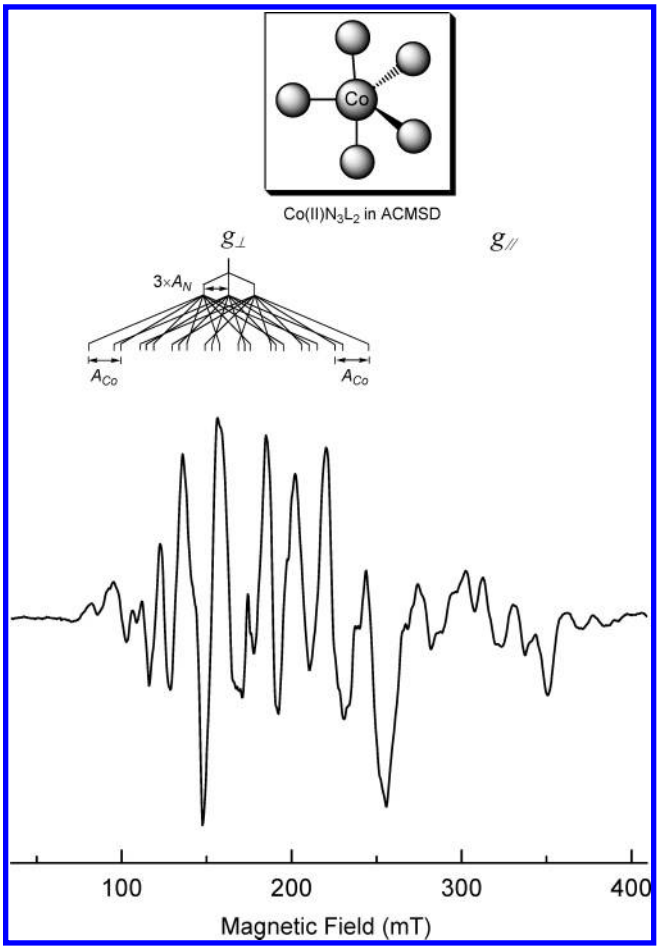

Figure 7. Calculated hyperfine splitting diagram for the $g_\perp$ region and the baseline corrected 4 K EPR spectrum of Co(II)-ACMSD. The inset shown on the top is a proposed trigonal-bipyramidal metal binding site. Three of the ligands are proposed to be endogenous nitrogens; the remaining two (L) are likely oxygens from either protein or solvent.

cobalt hyperfine structure became invisible. This is an interesting phenomenon for a cobalt ion in a protein matrix. The EPR signal line widths remain constant at 6−20 K although the signal intensity appears to be better observed at 10 K. Either at 4 or 10 K, the EPR signal was easily saturated by microwave power even at relatively low microwave power. The presented 4 K spectrum was obtained at 0.05 mW power with a severely distorted baseline, and it was in an absorption shape.

The hyperfine structures observed in the $g_\perp$ and at some extent in the $g_{||}$ regions are due to coupling of the spin of the electronic ground state with the ^{59}Co nuclear spin. Ideally, each principal g component should present eight equally spaced lines. But they do not occur in most of the chemical and biological systems. If observable, the ^{59}Co hyperfine couplings are often present only in one axial direction. In the 4 K ACMSD spectrum, the extensive hyperfine interactions are quite extensive. The splitting diagram is complex primarily because of the nearly axial pattern of the signal with overlapping spectral components, the complication of putative nitrogen contributions, i.e., superhyperfine couplings, and the easily saturated relaxation property. Based on the relative intensities observed in the low field wing of the spectrum, a ten-line splitting pattern is observed in the $g_\perp$ region. By using a perturbation theory based simulation algorithm (SimFornia), a spectrum with 10 lines of hyperfine splitting was predicted with the parameters given in Table 2 that were simulated from the 10 K EPR data (Figure 6). Again, the contributions of three nitrogen ligands were required for the simulation (Figure 7). Based on this understanding, the ten-line splitting pattern in $g_\perp$ region can be calculated using the hyperfine parameters given in Table 2. Figure 7 delineates such a prediction along with a baseline corrected experimental spectrum. Ultimately, the spectral assignments give strong support for a pentacoordinate ligand configuration at the cobalt center. Since $g_\perp > g_{||} > 2.0023$ and the ground state is assumed, a trigonal bipyramid structure is favored over tetragonal-pyramidal.[26]

On the other hand, we were not able to fully analyze the hyperfine ^{59}Co structure of the $g_{||}$ region. The EPR signal saturates at low microwave powers, and the signal intensities are relatively low for the hyperfine interactions at this direction. This region seems to be sensitive to both the ligand field and the protein environment (not shown). Further crystallographic and protein engineering studies may provide opportunities to elucidate the spectral importance of the $g_{||}$ region.

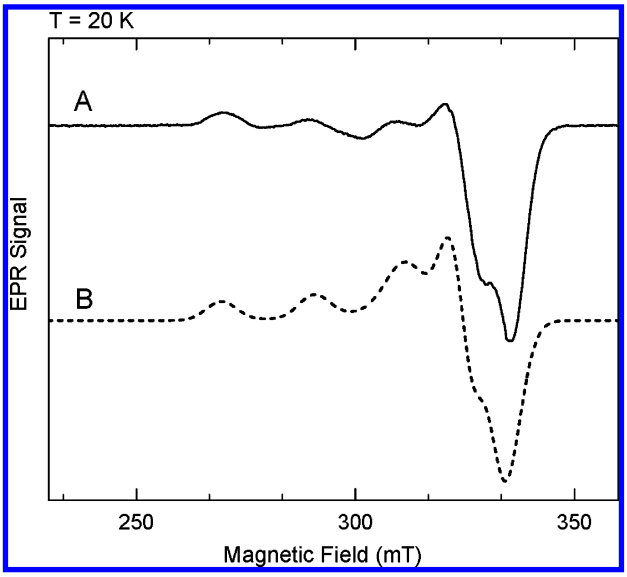

Figure 8. EPR spectrum of a copper(II)-substituted ACMSD at 20 K (A) and simulation (B). Spectrometer conditions: microwave frequency, 9.38 GHz; modulation amplitude, 0.3 mT; microwave power, 0.25 mW; time constant, 40.96 ms; and sweep time, 19.08 mT/s.

The EPR characterization on the active form of Co(II)-ACMSD has yielded clear evidence that the decarboxylase is a mononuclear metalloenzyme. If it were a binuclear metallocenter, either there should be no EPR signals for an antiferromagnetic coupling or the EPR spin quantitaion should present a 1:2 protein-to-metal ratio for an uncoupled case in the X-band perpendicular mode EPR spectrum.

EPR Characterization of Copper(II)-Substituted ACMSD. Our understanding of the electronic structure and ligand configuration of the ACMSD metal binding site is reinforced by EPR characterization of the Cu(II)-substituted ACMSD. A mononuclear Type II copper center with the expected total spin concentration was observed in these experiments (Figure 8). The copper nuclear spin ($I = {}^3/_2$) coupled to the electron spin and produced a hyperfine coupling of the EPR spectrum into four lines at the parallel region (A_z extracted from simulation: 189×10^{-4} cm^{-1}). The spin quantitation results indicate that the protein/metal stoichiometry is 1:1, i.e., only one metal ion bound at the enzyme active site. These observations exclude a thiolate−copper bond and tetrahedral geometry commonly seen in the Type I copper proteins, nor can a coupled binuclear (Type III) copper center be inferred from the EPR data. A small degree of rhombic distortion is presented in the EPR spectrum of the copper-substituted protein. Inasmuch as a different type of metal ion sits in the enzyme, this line of additional results corroborates the existence of a pentacoordinate mononuclear metal center in ACMSD with a mixed N/O ligand field in a low axial symmetry.

Discussion

Albeit the enzyme was first identified about four decades ago,[2−5] the mechanistic enzymology of ACMSD is still at its infancy. All previous experiments have indicated that ACMSD has no cofactor, not to mention any EPR spectroscopic characterization.[6,7] The fact that ACMSD can function as an iron(II) enzyme discovered in this study (Table 1) provides a rationale as to why the metal dependency was obscured in previous studies of several laboratories. ACMS, the substrate of the enzyme, is not commercially available owing to its instability. This compound nonenzymatically autocyclizes into **6**.[12] Thus the enzyme assay for ACMSD has to be coupled with a proceeding reaction catalyzed by the non-heme Fe(II)−enzyme HAD. In the enzyme purification process, a significant amount of Fe was lost from HAD. An excessive amount of Fe(II) was therefore included in the assay system in the prior studies.[6,7,9] In the present work, we used HAD as-is-isolated (or Fe/HAD 1:1 reconstituted) in the enzyme assay experiments. This precaution turned out to be a critical experimental detail in assessing ACMSD metal dependence.

The enzyme assay and steady-state kinetic experiments indicate that ACMSD of the 2-NBA biodegradation pathway utilizes a divalent metal for catalysis. The metal center of ACMSD is associated with both the enzyme specific activity and K_m, indicating that it plays an essential catalytic role and that there are complex interactions between the metal ion and the substrate. This finding is especially important in understanding the ACMSD mechanisms.

The EPR spectrum of a high-spin ($S = {}^3/_2$) Co(II) center is extremely sensitive to the coordination environment. It has been suggested that ^{59}Co hyperfine splitting is larger in high-spin octahedral and square pyramidal/trigonal-bipyramidal Co(II) centers and often observable in experiments, whereas hyperfine splitting of ^{59}Co tends to be relatively small in tetrahedral complexes and is easily smeared out by dipolar and exchange interactions.[27] The hyperfine splitting pattern in the ^{59}Co(II)-ACMSD EPR spectrum does not favor tetrahedral ligand geometry. The electronic spectrum and Co or Cu EPR data for ACMSD are consistent with numerous pentacoordinate, mixed nitrogen/oxygen ligands in either a square pyramidal or trigonal bipyramidal environment.[25,27]

The observed hyperfine structure at 4 K depends critically on the ground-state properties. Thus, the cobalt EPR parameters are not strong enough indicators alone to discriminate among four-, five-, and six-coordinates.[28,29] This limitation is remedied by the results obtained from two other observations. The copper-substituted ACMSD spectral features closely resemble the EPR spectra of some CuN_3O_2 complexes reported in the literature.[25] To ensure the reliability of the spectral analysis, the copper EPR spectrum has also been simulated (Table 2). Our confidence for the assignment of a pentacoordinate divalent metal is particularly reinforced by the empirical relationship between the maximum extinction coefficient of the visible $d-d$ band and the coordination number in cobalt(II) complexes. This relationship has been repeatedly confirmed to be a generally reliable rule-of-thumb.[29]

Together, our titration/assay, optical and EPR spectroscopic data lead to the conclusion that ACMSD is a metalloenzyme that possesses a mononuclear pentacoordinate divalent metal center at the active site. Since ACMSD from various origins share a high degree of sequence similarity, it is very likely that the enzyme in the tryptophan's kynurenine pathway is also a metalloenzyme. A multiple sequence alignment of the full-length

(27) Drago, R. S.; Stahlbush, J. R.; Kitko, D. J.; John, B. *J. Am. Chem. Soc.* **1980**, *102*, 1884−1889.
(28) Larrabee, J. A.; Alessi, C. M.; Asiedu, E. T.; Cook, J. O.; Hoerning, K. R.; Klingler, L. J.; Okin, G. S.; Santee, S. G.; Volkert, T. L. *J. Am. Chem. Soc.* **1997**, *119*, 4182−4196.
(29) Werth, M. T.; Tang, S.-F.; Formicka, G.; Zeppezauer, M.; Johnson, M. K. *Inorg. Chem.* **1995**, *34*, 218−228.

Table 3. Cofactor Dependency of Characterized Decarboxylases in Biology

cofactor	representing enzyme	refs
biotin	oxaloacetate decarboxylase	37
flavin	4-phosphopantethenoyl cysteine decarboxylase	38
$NAD^+/NADP^+$, and divalent ion activator	malic enzymes; methylmalonyl CoA decarboxylase	39, 40
pyridoxal 5′-phosphate	glycine decarboxylase; ornithine decarboxylase; DOPA decarboxylase	41, 42 43
pyruvoyl	arginine/aspartate/histidine decarboxylase; *S*-adenosylmethionine decarboxylase	44, 45 46, 47
thiamin pyrophosphate	pyruvate dehydrogenase complex (E1 decarboxylase); phosphonopyruvate decarboxylase	48
Fe(II), O_2 (oxidative)	gallic acid decarboxylase; CloR decarboxylase; αKG-dependent dioxygenases	49, 50 51, 52
Mn(II), O_2 (oxidative)	oxalate decarboxylase	53−55
M(II) (M = Fe, Co, Cd, or Mn)	α-amino-β-carboxy-muconic-ϵ-semialdehyde decarboxylase (ACMSD)	this work

ACMSD protein sequences has shown that four histidine residues (i.e., His-9, His-11, His-177, and His-228) and eight aspartate/glutamate residues are strictly conserved across ACMSD sequences (Figure S2). This conservation warrants that the decarboxylase has sufficient endogenous residues for an N_3O_2 ligand donor field predicted from the EPR spectral assignment. To further identify the metal ligands and probe the active site architecture, a comprehensive site-directed mutagenesis study and corresponding spectroscopic characterizations have been initiated. Due to the instability of the immediate substrate and product, characterizing a catalytically competent enzyme−substrate complex remains a challenge. Nevertheless, the present work opens an avenue for characterization of the putative binary complex using metal ions that are not active at the active site, even though it is unclear whether such a complex would reflect that of the catalytic intermediates. EPR spectroscopy may be amenable for continued studies on this enzyme.

Several divalent metal ions can activate the bacterial ACMSD, but due to low metal binding affinity, it is not yet possible to identify the physiologically relevant metal cofactor. The Co(II)-ACMSD appears to be an ideal catalyst in vitro because of its stability and higher substrate turnover number. But this does not necessarily suggest that ACMSD is a cobalt enzyme in vivo. We conducted some of the experiments with cobalt(II)-supplemental medium for the purpose of spectroscopic characterizations and for avoiding complications due to the reconstitution reaction. The observation that the *E. coli* cells can uptake Co(II), transport, and incorporate it into the enzyme active site during cell growth is intriguing. Although cobalt transporters have been identified in some systems,[30] very few noncorrinoid cobalt-containing enzymes have been identified,[31] some of which are still controversial.[32−34] The question of native metal identity has been a general problem for members of several enzyme superfamilies when either Co(II) or other divalent metal ions can be used as a cofactor.[35] Further studies will be needed to clarify the native metallocofactor.

It is intriguing that ACMSD can utilize several divalent metals including Fe, Co, Cd, and Mn to operate the nonoxidative decarboxylation chemistry. The enzyme appears enzymatically inactive when a copper ion occupies the metal binding site. The rational basis as to why, for the same ligand donor field and protein architecture, different metal ions afford different catalytic efficiencies in this enzyme remains unclear. A similar property has been observed in many other systems, particularly those zinc-dependent enzymes.[35] The catalytic competence and efficiency may stem directly from the redox properties of the metal ion and subtle coordination differences such as bond lengths and angles at the enzyme active site.

Decarboxylation reactions are among the most common biological and chemical transformations.[36] Nature has evolved a wide variety of catalytic strategies to remove a carboxyl group from organic chemicals for a variety of purposes (Table 3). Despite substantial understandings, new mechanisms are continuously being discovered. In general, nonoxidative decarboxylation is poorly understood in both prokaryotes and eukaryotes relative to the oxidative decarboxylation.[36] The finding of a metal cofactor for ACMSD is a significant advance that will shed light on further mechanistic understanding of nonoxidative decarboxylations of this type. To the best of our knowledge, a non-heme, noncorrinoid, divalent metal center at the active site of a nonoxidative decarboxylase has never been reported (Table 3). Thus, the catalytic reaction of ACMSD, important in at least two unrelated metabolic events, represents an unprecedented decarboxylation mechanism deserving of further chemical and spectroscopic study.

Acknowledgment. This work was supported in part by funds from the ORAU Faculty Enhancement Award in Life Sciences

(30) Komeda, H.; Kobayashi, M.; Shimizu, S. *Proc. Natl. Acad. Sci. U.S.A.* **1997**, *94*, 36−41.
(31) Kobayashi, M.; Shimizu, S. *Eur. J. Biochem.* **1999**, *261*, 1−9.
(32) D'Souza, V. M.; Holz, R. C. *Biochemistry* **1999**, *38*, 11079−11085.
(33) Walker, K. W.; Bradshaw, R. A. *Protein Sci.* **1998**, *7*, 2684−2687.
(34) Wang, J.; Sheppard, G. S.; Lou, P.; Kawai, M.; Park, C.; Egan, D. A.; Schneider, A.; Bouska, J.; Lesniewski, R.; Henkin, J. *Biochemistry* **2003**, *42*, 5035−5042.
(35) Lipscomb, W. N.; Sträter, N. *Chem. Rev.* **1996**, *96*, 2375−2433.
(36) O'Leary, M. H. *Enzymes (3rd ed.)* **1992**, *20*, 235−269.
(37) Jitrapakdee, S.; Wallace, J. C. *Curr. Protein Pept. Sci.* **2003**, *4*, 217−229.
(38) Rangarajan, E. S.; Li, Y.; Iannuzzi, P.; Tocilj, A.; Hung, L. W.; Matte, A.; Cygler, M. *Protein. Sci.* **2004**, *13*, 3006−3016.
(39) Yang, Z.; Zhang, H.; Hung, H. C.; Kuo, C. C.; Tsai, L. C.; Yuan, H. S.; Chou, W. Y.; Chang, G. G.; Tong, L. *Protein. Sci.* **2002**, *11*, 332−341.
(40) Karsten, W. E.; Tipton, P. A.; Cook, P. F. *Biochemistry* **2002**, *41*, 12193−12199.
(41) Perham, R. N. *Annu. Rev. Biochem.* **2000**, *69*, 961−1004.
(42) Grishin, N. V.; Osterman, A. L.; Brooks, H. B.; Phillips, M. A.; Goldsmith, E. J. *Biochemistry* **1999**, *38*, 15174−15184.
(43) Burkhard, P.; Dominici, P.; Borri-Voltattorni, C.; Jansonius, J. N.; Malashkevich, V. N. *Nat. Struct. Biol.* **2001**, *8*, 963−967.
(44) Tolbert, W. D.; Graham, D. E.; White, R. H.; Ealick, S. E. *Structure* **2003**, *11*, 285−294.
(45) Gallagher, T.; Snell, E. E.; Hackert, M. L. *J. Biol. Chem.* **1989**, *264*, 12737−12743.
(46) Hillary, R. A.; Pegg, A. E. *Biochim. Biophys. Acta* **2003**, *1647*, 161−166.
(47) Tolbert, W. D.; Zhang, Y.; Cottet, S. E.; Bennett, E. M.; Ekstrom, J. L.; Pegg, A. E.; Ealick, S. E. *Biochemistry* **2003**, *42*, 2386-2395.
(48) Zhang, G.; Dai, J.; Lu, Z.; Dunaway-Mariano, D. *J. Biol. Chem.* **2003**, *278*, 41302−41308.
(49) Zeida, M.; Wieser, M.; Yoshida, T.; Sugio, T.; Nagasawa, T. *Appl. Environ. Microbiol.* **1998**, *64*, 4743−4747.
(50) Pojer, F.; Kahlich, R.; Kammerer, B.; Li, S.-M.; Heide, L. *J. Biol. Chem.* **2003**, *278*, 30661−30668.
(51) Prescott, A. G.; Lloyd, M. D. *Nat. Prod. Rep.* **2000**, *17*, 367−383.
(52) Hausinger, R. P. *Crit. Rev. Biochem. Mol. Biol.* **2004**, *39*, 21−68.
(53) Anand, R.; Dorrestein, P. C.; Kinsland, C.; Begley, T. P.; Ealick, S. E. *Biochemistry* **2002**, *41*, 7659−7669.
(54) Chang, C. H.; Svedruzic, D.; Ozarowski, A.; Walker, L.; Yeagle, G.; Britt, R. D.; Angerhofer, A.; Richards, N. G. *J. Biol. Chem.* **2004**, *279*, 52840−52849.
(55) Reinhardt, L. A.; Svedruzic, D.; Chang, C. H.; Cleland, W. W.; Richards, N. G. *J. Am. Chem. Soc.* **2003**, *125*, 1244−1252.

(A.L.), University of Mississippi Medical Center New Faculty Start-up Funds (A.L.), and Mext. Haiteku (2002-2006) (Y.H.). We thank Mr. Ben Brock (UMMC) for reading the manuscript and suggesting pertinent changes.

Supporting Information Available: Simulation details for the discussed cobalt and copper EPR spectra (Table S1 and S2), a screenshot of the theoretical predictions of the cobalt hyperfine interactions at the $g_{\perp}$ region (Figure S1), and a multiple sequence alignment of ACMSD protein sequences (Figure S2). This material is available free of charge via the Internet at http://pubs.acs.org.

JA0532234

Kinetic and Spectroscopic Characterization of ACMSD from *Pseudomonas fluorescens* Reveals a Pentacoordinate Mononuclear Metallocofactor

Tingfeng Li,[‡] Antoinette L. Walker,[‡] Hiroaki Iwaki,[§] Yoshie Hasegawa,[§] and Aimin Liu*[‡]

[‡]Department of Biochemistry, University of Mississippi Medical Center, Jackson, MS 39216-4505, and [§]Department of Biotechnology, Faculty of Engineering, Kansai University, Suita, Osaka 564-8680, Japan

Title Running Head: **ACMSD is a Metalloenzyme**

* Corresponding Author: Tel: 601-984-1872, Fax: 601-984-1501, and E-mail: aliu@biochem.umsmed.edu

[‡] University of Mississippi Medical Center

[§] Kansai University

Supporting Information (6 pages)

Table S1. Input File for the Spectral Simulation of Co-ACMSD at 10 K.

```
#
# Simulation of the as-is-isolated high spin Cobalt ACMSD at 10 K
#

OUT    =  "ACMSDHS10K_sim.OUT";
ITOT   =  1.6e8;

NEW_SPECIES = "CoACMSD"   1.00;

 Freq   = 9.384;
 Hmin   = 1;
 Hmax   = 5001;
 NDATA  = 1024;

 S  = 1.5;
 gx = 2.613;
 gy = 4.634;
 gz = 4.7622;
 Wx = 166.76;
 Wy = 232.58;
 Wz = 486.57;

 Shape  = 2;
 CutOff = 15;
 WidthMode = 2;
 TMIN   = 0.00;
 TMAX   = 360.00;

 NT     = 360;
 PMIN   = 0.00;
 PMAX   = 90.00;
 NP     = 180;
 T     = 10.0;

# cobalt parameters
 NUMNUCLEI = 1;
 Spin[0]   = 3.5;
 Num[0]    = 1;
 SecondOrder[0]= 0;
 ISTP[0]   = 1;
 gnRatio[0]= 1.00000;
 Abund[0]  = 1.0;
 AX[0]     = 30.6; # in MHz
 AY[0]     = 29.6;
 AZ[0]     = 339.4;
 ALPHAA[0] = 45.00;
 BETAA[0]  = 6.00;
 GAMMAA[0] = 0.00;

 C2X[0]   = 5.50;
 C2Y[0]   = 5.5;
 C2Z[0]   = 5;
 EX[0]    = -0.04700;
 EY[0]    = 0.047;
```

```
 EZ[0]    = -0.0001;

# Lower Nitrogen ligand (3 equiv.)
 NUMNUCLEI = 3;
 Spin[1]   = 1;
 Num[1]    = 3;
 SecondOrder[1]= 0;
 ISTP[1]   = 1;
 gnRatio[1]= 1.00000;
 Abund[1]  = 1.0;
 AX[1]     = 26.3;
 AY[1]     = 16.7;
 AZ[1]     = 79.1;
 ALPHAA[1] = 45.00;
 BETAA[1]  = 6.00;
 GAMMAA[1] = 0.00;

END;
```

Table S2. Input File For Spectral Simulation of Cu-ACMSD.

```
#
# Simulation of Cu(II)-ACMSD at 20 K
#
OUT    = "ACMSD_Cu20KSim.out";
ITOT   = 6e8; # the total double integral for the final spectrum

NEW_SPECIES = "CuN3O2"  1.00;

 Freq   = 35.384;
 Hmin   = 2130.00;
 Hmax   = 3730.00;
 NDATA  = 1024;

 S      = 0.5;
 gx     = 2.0677;
 gy     = 2.0732;
 gz     = 2.2385;
 Wx     = 33.54;
 Wy     = 41.52;
 Wz     = 43.29;

 Shape    = 2;
 CutOff   = 4;
 WidthMode= 1;
 TMIN     = 0.00;
 TMAX     = 90.00;
 NT       = 90;
 PMIN     = 0.00;
 PMAX     = 90.00;
 NP       = 0;
 T        = 20.0;
```

```
 NUMNUCLEI = 1;   # Cu(II)
 Spin[0]   = 1.5;
 Num[0]    = 1;
 SecondOrder[0]= 1;
 ISTP[0]   = 1;
 gnRatio[0]= 1.07000;
 Abund[0]  = 0.5;
 AX[0]     = 30.00;
 AY[0]     = 128.00;
 AZ[0]     = 568;
 C2X[0]    = 0.00;
 C2Y[0]    = 0.00;
 C2Z[0]    = 15.00;
 EX[0]     = 0.00;
 EY[0]     = 0.00;
 EZ[0]     = -0.05;

 NUMNUCLEI = 3;  # Nitrogen
 Spin[1]   = 1;
 Num[1]    = 3;
 SecondOrder[1]= 0;
 ISTP[1]   = 1;
 gnRatio[1]= 1.00000;
 Abund[1]  = 1.00000;
 AX[1]     = 20.00;
 AY[1]     = 20.00;
 AZ[1]     = 25.00;
 ALPHAA[1] = 0.00;
 BETAA[1]  = 0.00;
 GAMMAA[1] = 0.00;
 C2X[1]    = 0.00;
 C2Y[1]    = 0.00;
 C2Z[1]    =  0.00;
 EX[1]     = -0.0002;
 EY[1] =  -0.0002;
 EZ[1] = 0.00;


END;
```

Figure S1. A Screenshot of the SimFonia Predictions Using the *g* and *A* Principal Values from the Spectral Simulation at 10 K (Table 2).

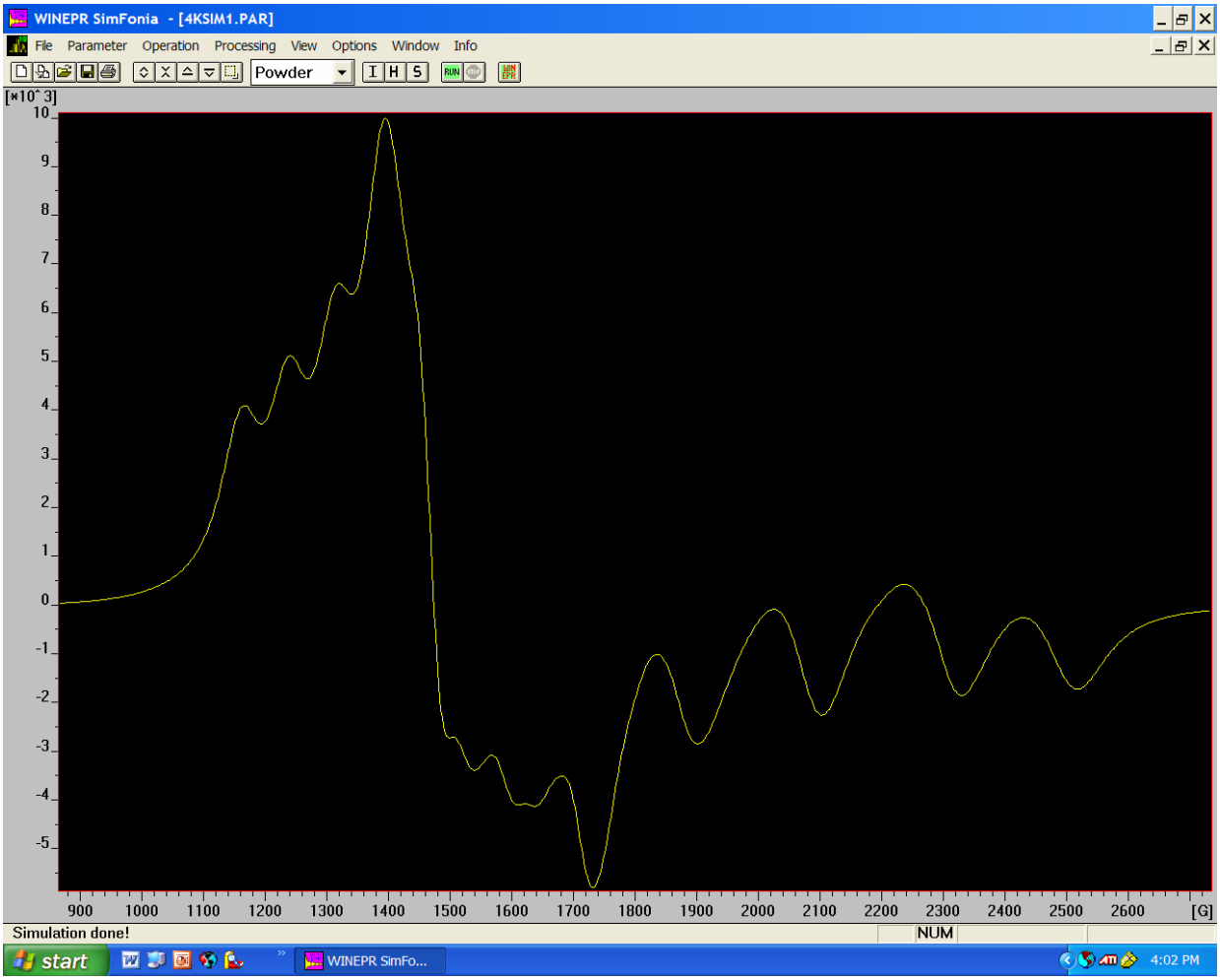

Figure S2. Multiple Sequence Alignment of Representative ACMSD Protein Sequences.

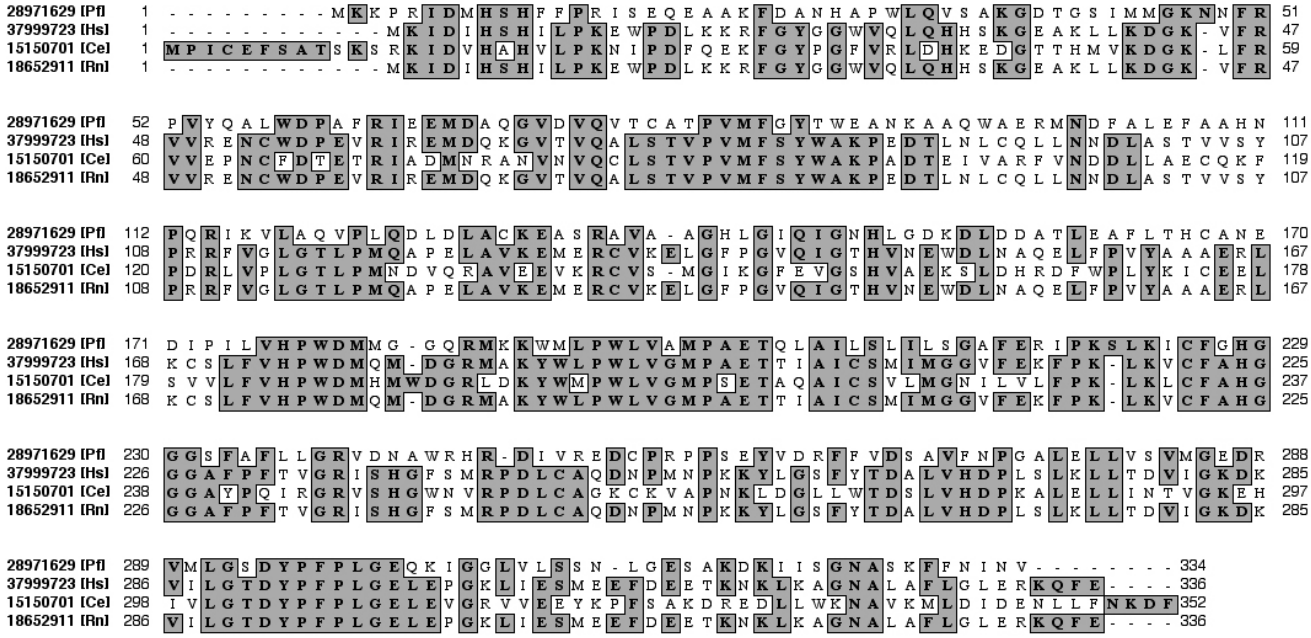

Sequences are labeled according to the NCBI gene identification (gi) number and species name. Abbreviations of species names are: Pf, *Pseudomonas fluorescens*; Hs, *Homo sapiens*; Ce, *Caenorhabditis elegans*; Rn, *Rattus norvegicus*.